doi:10.14311/ppt.2024.1.28
Plasma Physics and Technology **11**(1):28–35, 2024

ELECTRICAL MODELS OF ARCS IN DIFFERENT APPLICATIONS

D. Uhrlandt[a,b,*], A. Najam[a], G. Gött[a], R. Methling[a], M. Baeva[a], S. Gortschakow[a], D. Gonzalez[a]

[a] *Leibniz-Institute for Plasma Science and Technology, Felix-Hausdorff-Str. 2, 17489 Greifswald, Germany*

[b] *Institute for Electrical Power Engineering, University of Rostock, Tannenweg 22, 18059 Rostock, Germany*

[*] uhrlandt@inp-greifswald.de

Abstract. The electrical characteristic of arcs sensitively depends on many factors like electrode material and shape, working gas and gas pressure. Arc sheath voltages and electrode resistance have to be considered in particular for shorter arcs. The arc voltage behaviour is important to the switching performance. But its knowledge also allows to estimate the power consumption of the arc and the heat transferred to the electrodes. Arc voltage models are easy to integrate in power grid simulations and benefitial for the design of arc power sources. Whereas specific arc voltage models are available meanwhile for many examples, there are still knowledge gaps for arcs in a wide range of parameters. This paper provides a review of recently developed electric arc models for high and low voltage switching as well as for welding with the focus on vacuum arcs, short arcs and arcs at low current.

Keywords: electric arc model, switching arc, welding arc, vacuum arc.

1. Introduction

The prediction of arc properties by models has been established in many applications as a prerequisite for the design of the arc electrode configuration, the power sources or the adaption of the corresponding processes. First principle models as e.g. fluid models or magnetohydrodynamic models are increasingly used because of their ability to analyse the physical mechanisms in detail. These models need a high number of input data such as thermophysical, transport and radiation data. Moreover, assumptions concerning thermodynamic equilibrium, compressibility, turbulence, optically thin radiation and others are required. Therefore, and indepth validation by measurements is recommended also for this kind of models.

In contrast, electrical models of arcs or so-called black-box models are much simpler and easy to implement. However, they typically include parameters, which have to be deduced froma sufficient number of measurements in the corresponding operation range. In fact, these models result mainly from fitting of electrical measurements such as the arc voltage characteristics dependent on current. Their validity is limited to the specific arc configuration and the operation range of the particular measurements. Nevertheless, electric arc models have a long history and can be very beneficial even for complex arc applications, where a detailed physical model is difficult to develop or hardly affordable.

This paper is aimed at a short introduction into electric arc models of different kind, the illustration of their specification and use in applications with a more complex arc behaviour by examples, and providing recent results for arc models in specific cases of short arcs at low current and arcs at higher pressure.

Electric arc models can be classified into two groups. The first group compraises models of the time-dependent arc conductivity e.g. in alternating current (AC) applications. The second group involves models of the instantaneous voltage dependent on current and other changing quantities like the arc length. Although there is obviously a way to transfer a model from one into the other group, they should be considered separately as it was done also in their history.

The first group is based on a general physical approach considering the energy stored in an arc as a result of power gain and power loss over time. This energy defines the arc conductance $g(t)$ over time t. Considering the instant power gain as the product of voltage $u(t)$ and current $i(t)$, the power balance results in a presentation of the temporal conductivity behaviour as

$$\frac{1}{g}\frac{\mathrm{d}g}{\mathrm{d}t} = \frac{1}{\tau}\left(\frac{ui}{P_{\mathrm{loss}}} - 1\right) \tag{1}$$

first given by Mayr [1] in 1943. In equation (1), P_{loss} and τ are a cooling constant and the arc time, respectively. The equation is mainly based on the assumption of a cylindrical arc of constant diameter and a dominant radial heat transport. It is typically applied in the low current range, e.g. near current zero in switching applications. Otherwise, assuming a cylindrical arc of constant temperature in space and time but letting the arc diameter change, a similar approach leads to a model with the same equation (1) but replacing the constant P_{loss} by a variable function $P_{\mathrm{loss}}(t) = u_{\mathrm{av}}|i|$. Here, u_{av} is the average voltage over time. This model has been proposed by Cassie [2] already in 1939, and it turned out to be better applicable for higher currents as e.g. in the high-current

range of switching arcs.

Based on these approaches, many authors have deduced more sophisticated versions typically with more fitting parameters to get more accurate results for specific arc configurations. This has been done in particular by the introduction of further functional dependencies e.g. considering $\tau(t) = \tau_0 g(t)^\alpha$ and $P_{\text{loss}}(t) = P_0 g(t)^\beta$ with constant parameters τ_0, P_0, α, and β by Schwarz [3] or considering $P_{\text{loss}}(t) = \max(u_{\text{av}}|i|, P_0 + P_1 ui)$ with an additional cooling constant P_1 by Schavemaker et al. [4]. The interesting issue of these versions is that they contain the Mayr and the Cassie approach as specific cases and provide good approximations for both low and high voltages.

The second group of electric models is originally based on the considerartion of direct current (DC) arcs. These models typically define the instant value of the arc voltage u as a function of the arc current i and other quantities like the gap distance or arc length l_{arc}. Corresponding models have been deduced very early as for example by Ayrton (1902) [5], Steinmetz (1906) [6], and Nottingham (1923) [7]. The expression of Ayrton

$$u = U_0 + E_0 l_{\text{arc}} + \frac{P_0 + P_1 l_{\text{arc}}}{i} \tag{2}$$

with the fit parameters U_0 (voltage constant), E_0 (electric field constant), P_0 (power constant), and P_1 (power gradient constant) is given here to show the general structure of such models.

Subsequently, specified and more sophisticated electric arc models of both kinds have been developed for many applications. As examples of the first group, the work of Smeets et al. [8] proposing the later on called KEMA model, which consists of a series of Mayr models appropriate for the current zero range in high-voltage breaker, and the review of three different arc models for high-voltage breakers in [9] can be mentioned. For the second group, the review of Ammerman et al. [10] can be pointed out.

In the next two sections, specifc features of electric arc models of both groups are illustrated by examples of recently developed models. This comprises models for quite different applications like vacuum arcs in medium-voltage current breakers, experimental arcs to study electrode erosion in high-voltage circuit breakers, an example for gas metal arc welding as well as low-voltage switching.

2. Improved models for AC arcs

Electric model of a vaccum arc A vacuum switching arc is considered in order to illustrate how an AC arc with specific changes of the arc voltage can be successfully simulated. In [11] an arc in a vacuum interrupter (VI) was considered. Instead of a real VI, a model switch in a vacuum chamber with optical access has been used to study the arc. Cylindrical contacts made of typical copper-chromium alloys with

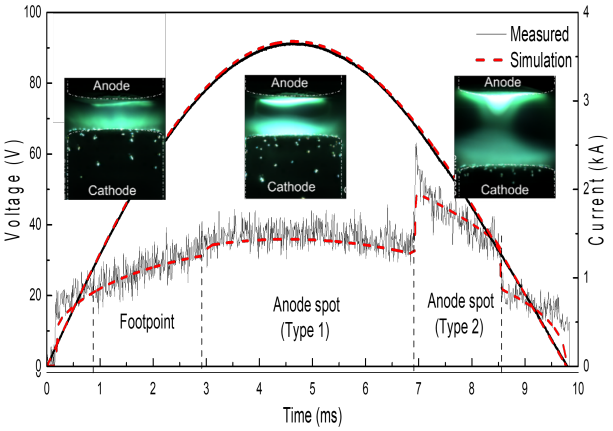

Figure 1. Voltage and current from measurements and the electric model for a vacuum switching arc with the peak current 3.6 kA.

25 % copper and a diameter of 10 mm have been separated with a speed of 1 m/s providing a gap distance of up to 9 mm in a half period of the AC current. The model switch is operated with AC currents at 50 Hz up to a peak current of 4.6 kA. Because of the relatively small contact diameter, current densities of up to $5{\cdot}10^7$ A/m^2 have been obtained. Considering typical short circuit currents in interrupters at 12 kV rated voltage with axial magnetic field (AMF) contacts [12], contact diameters of 100 mm are proposed for 110 kA peak current. Hence, current densities up to about $1.4{\cdot}10^7$ A/m^2 arise in real applications, and the model switch experiments are suited to study upper limits of switching applications. At these limits specific phenomena occur at the anode. The so called high-current anode spot modes develop depending on current, arcing time, and gap distance. Whereas the arc starts typically in a diffuse mode, first a footpoint mode is established followed by an anode spot type 1 and, if the current is high enough, followed by an anode spot type 2. The mode changes are accompanied by sudden jumps in the arc voltage due to fundamental changes in the arc-anode interaction. Such mode changes should be avoided in the real application because they promote contact evaporation and lower the insulation strength after current zero (CZ). Hence, an electric model is useful for the control of larger parameter ranges to forecast the breaker performance. Therefore, the equation given in [4] have been modified and used in the form:

$$\frac{1}{g}\frac{\mathrm{d}g}{\mathrm{d}t} = \frac{1}{cv}\left(\frac{ui}{(U_h(1-at)+U_d)|i|^b} - 1\right) \tag{3}$$

where t is the time in the current period, v is the contact speed with a fit coefficient c, U_d is the arc voltage in the diffuse mode, and a and b are calibration constants. A voltage offset is considered as

$$\begin{aligned} U_h \;=\; & U_{h1}\left[u_s(t-t_0) - u_s(t-t_1)\right] \\ & + U_{h2}\left[u_s(t-t_2) - u_s(t-t_3)\right] \end{aligned} \tag{4}$$

where U_{h1} and U_{h2} represent the additional voltages in the high-current anode modes, t_0, t_1, t_2, and t_3 are the onset and offset times of the modes, and u_s is a step function (see [11] for further details). Obviously, the times, the voltages U_d, U_{h1}, U_{h2} and the coefficients a, b and c must be adapted appropriately with measurements. This has been done in [11] using several experiments with different currents and arcing times. The borders of the mode changes have been identified in particular, and the model could be validated in quite different situations. An example is given in Figure 1 where the measured and simulated voltage and current courses can be seen together with some high-speed camera images of the corresponding arcs in anode spot modes.

Electric model including the power balance Another example illustrates how electrical models can be combined with considerations of the arc physics and geometry. Starting again with the general approach for deducing the models of the first group, the energy stored in the arc can be considered and the arc can be assumed to be a cylindrical homogeneous plasma. But in contrast to other models, the time dependent power balance can be included in a more general form. The electric model in [13] considers the arc conductance as dependent on the total power P_{total} in the form

$$g(t) = \frac{i(t)^2}{P_{\mathrm{total}}(t)} \qquad (5)$$
$$P_{\mathrm{total}} = P_{\mathrm{rad}} + P_{\mathrm{tur}} + P_{\mathrm{ramf}} + P_{\mathrm{axmf}} + P_{\mathrm{net}}$$

with the radiative power loss $P_{\mathrm{rad}} = 2\pi^2 r_{\mathrm{arc}}^2 l_{\mathrm{arc}} \epsilon_N$, the turbulent power loss $P_{\mathrm{tur}} = k_{\mathrm{tur}} h_{\mathrm{arc}} \rho_{\mathrm{arc}} l_{\mathrm{arc}} r_{\mathrm{arc}} v_{\mathrm{sound}}$, the power gain $P_{\mathrm{axmf}} = k_{\mathrm{axmf}} \dot{m}_{\mathrm{ax}} h_{\mathrm{arc}}$ by the axial mass flow from the electrodes, the power loss $P_{\mathrm{ramf}} = k_{\mathrm{ramf}} \dot{m}_{\mathrm{rad}} h_{\mathrm{av}}$ by the radial mass flow, and net change $P_{\mathrm{net}} = k_{\mathrm{net}} l_{\mathrm{arc}} \left[\frac{\mathrm{d}}{\mathrm{d}t}(\rho_a r c A_{\mathrm{arc}} h_{\mathrm{arc}}) - \dot{p}_{\mathrm{arc}} A_{\mathrm{arc}}\right]$. Here, r_{arc}, A_{arc}, and l_{arc} are the arc radius, cross section and length, respectively. ρ_{arc}, p_{arc}, and h_{arc} are the mass density, pressure, and enthalpy, respectively, and h_{av} is the temporally averaged enthalpy in the arc, v_{sound} the speed of sound, ϵ_N the radiation net emission coefficient, and $\dot{m}_{\mathrm{ax}}$ and $\dot{m}_{\mathrm{rad}}$ the axial and radial mass flows. k_{tur}, k_{axmf}, k_{ramf}, and k_{net} have been introduced as fitting coefficients. The model is based mainly on the approach given in [9] with a modification of the radiation term, in particular.

The model was applied in [13] to an arc at atmospheric conditions between cylindrical copper-tungsten electrodes. Using electrodes of 10 mm in diameter confined by ceramic tubes and applying an AC current at 50 Hz with a peak current of 1.5 kA, current densities of about 10^7 A/m^2 at the electrode surfaces have been generated. These experimental conditions have been chosen to simulate the arc behaviour near the electrodes in gas circuit breakers. A strong copper evaporation results from the high current densities and dominates the arc properties [14]. To determine the large number of unknown quantities in the model, measurements of voltage and current have been complemented by optical and spectroscopic investigations. Like in other models, the determination of the arc radius is very important [15]. The temporal variation has been fitted in [13] by the expression $2r_{\mathrm{arc}}(t) = b|i(t)|^q$, and the parameters b and q have been fixed by the help of high-speed images of the arc. Spectroscopic studies and spectrum simulations have been used to estimate the arc temperature in a range between 14 and 16 kK. The physical quantities such as v_{sound} and ϵ_N have been estimated assuming a pure copper vapour, because the properties of copper are dominant in this temperature range. Temporal changes have been considered to be dependent on the current magnitude in particular for the pressure with $p_{\mathrm{arc}}(t) = p_0 + k_p|i(t)|$ and fitting parameters p_0 and k_p. In addition, the simple relations $A_{\mathrm{arc}} = \pi r_{\mathrm{arc}}^2$, $\rho_{\mathrm{arc}} = k_p p_{\mathrm{arc}}$, $h_{\mathrm{arc}} = h_0 - k_h p_{\mathrm{arc}}$, $\dot{m}_{\mathrm{ax}} = A_{\mathrm{arc}} \rho_{\mathrm{arc}} v_{\mathrm{sound}}$, $\dot{m}_{\mathrm{rad}} = A_{\mathrm{arc}}(\dot{\rho}_a r c l_{\mathrm{arc}} + \rho_{\mathrm{arc}} v_{\mathrm{sound}})$ are used. Finally, 9 fitting constants remained open and have been adapted by experiments and measurements of current and voltage.

An example of the results is illustrated in Figure 2. The benefit of the model is not only an appropriate prediction of the voltage behaviour but also the estimation of main power loss chanels and their changes over time. The radiation term followed by the radial mass flow term are the most important parts in the arc power budget.

More sophisticated electrical models can be obtained when considering the power balance in form of a partial differential equation. An example is the solution of the Elenbass-Heller equation, which has been used e.g. by Guye et al. [16].

3. Models dependent on arc length

This section is aimed at illustrating recent studies on electric arc models of the second group, in particular for arcs of short length where voltage drops over the electrodes and the electrode sheath voltages contribute considerably to the measured total arc voltage in the configuration. These contributions are often neglected in former models which focus on the arc column and are not applicable in the range of contact opening or around short circuiting.

Electric model of an arc welding process The first example of a very detailed study concerns gas metal arc welding (GMAW) which has a broad application range for high efficient joining of mild or stainless steel and just recently also for additive manufacturing. Here, the workpiece with the molten weld pool acts as the cathode, and the steel wire fed through a contact tube in the welding burner is the anode. Due to the arc, the tip of the wire anode is molten and builds droplets, which are transferred to the weld pool. A shielding gas is fed through a ceramic nozzle of the burner, which cools the anode and screens the arc and the weld pool against ambient air. As a quite stable

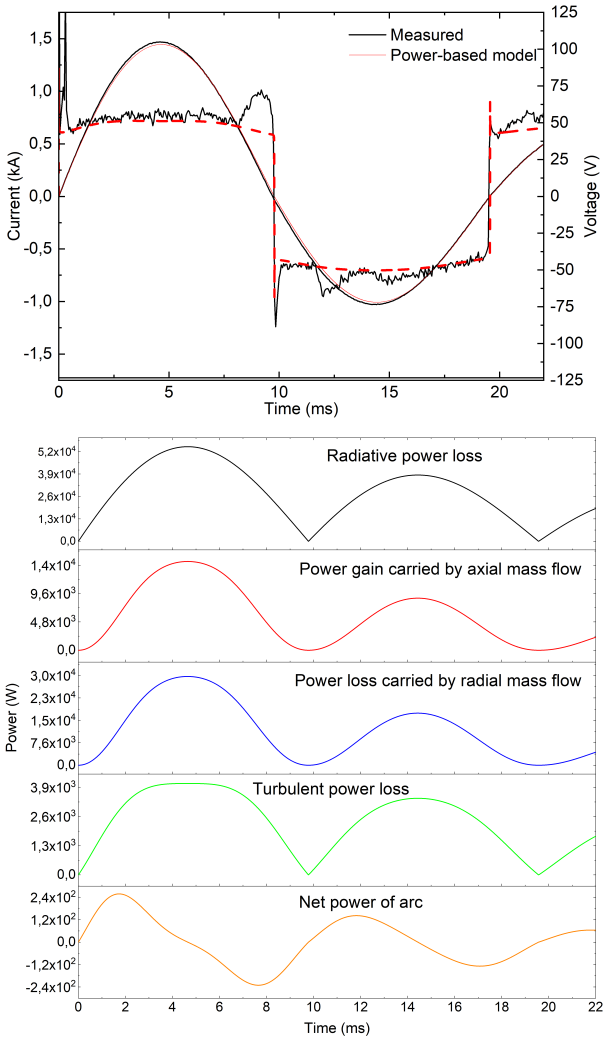

Figure 2. Voltage and current from measurements and the electric model as well as temporal variation of main contributions of the arc power balance for a copper vapour dominated arc with the peak current 1.5 kA at atmospheric conditions.

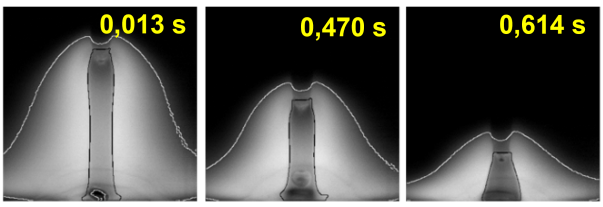

Figure 3. Combination of high speed images of the central and the outer part of the arc at three times in the pulse period of a GMAW process.

process mode, pulsed GMAW with one drop per pulse is considered here. Such a process typically uses DC voltage with a pulse period of several milliseconds and several hundreds of A followed by a longer base period of several tens of A.

Experimental and numerical studies of the arc in such a process have confirmed a specific structure of the arc with a strong flow from the anode side

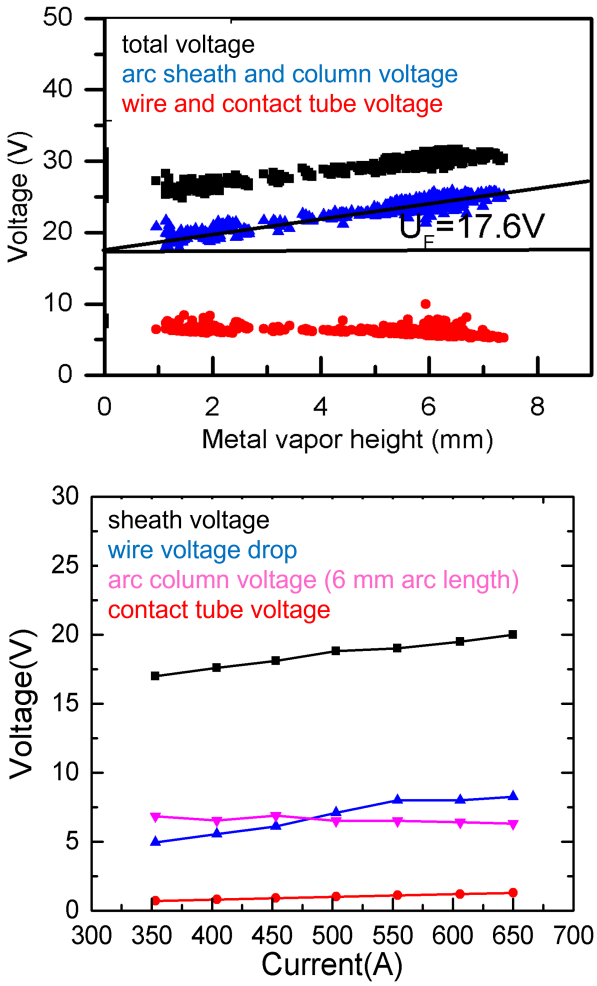

Figure 4. Voltages for different arc lengths in the pulse period for the pulse current of 400 A (upper part) and voltage drops along the current path dependent on the pulse current (lower part).

to the cathode, a central part dominated by metal vapour coming from the hot wire tip and an outer part dominated by the shielding gas. At least in the case of argon shielding gas, the arc temperature in the metal vapour core is by several thousands of K lower than in the shielding gas part [17]. As a consequence, the main part of the current flows from outer regions of the weld pool through the region around the metal vapour core to the upper shoulder of the molten wire tip. This has to be considered in an arc length estimation.

The typical arc structure for different times in the pulse is illustrated in Figure 3, where pictures are constructed from two high speed images with spectral filters and different intensity of the metal vapour dominated inner part and the outer part of the arc in the shielding gas.

The arc voltage in a GMAW process is typically measured between the burner and the workpiece. Whereas a larger steel workpiece has a comparatively low resistance, the contribution of the wire system to the total resistance is considerable. One important part is the contact resistance in the contact tube, where the

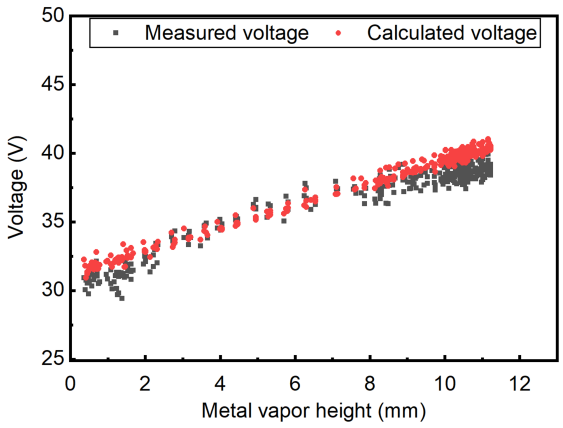

Figure 5. Comparison of the model results with voltage measurements from many experiments for different arc lengths for the case of a pulse current of 550 A.

wire passes through. In addition, the steel wire with a specific temperature distribution up to the molten tip leads to a corresponding voltage drop. Extensive studies including pyrometric measurements of the wire temperature distribution, short circuit measurements and separate studies of the temperature dependence of the wire conductivity [18] provided the wire and contact tube resistance in the considered pulsed GMAW process in dependence of the pulse current. These results have been combined in further studies with measurements of the voltage together with an optical analysis of the arc and electrode structure leading to estimations of the current path length [19]. Plotting the difference of the measured total voltage and the voltage drop in the wire and contact tube over the current path length, an almost linear dependence has been found. A linear fit yielded the sheath voltage (the value for vanishing arc length) and the averaged electric field in the arc column for the arc in the pulse period for different pulse currents. This is illustrated in Figure 4 (upper part) for the case of a pulse current of 400 A. In the lower part of the figure, the respective voltage drops are plotted as functions of the pulse current. The sum of the voltage drops over the cathode and anode sheath represents by far the largest contribution and leads to the main power input into the process.

In a next work [20], the studies have been extended, and an electric arc model for the arc in the pulse period have been deduced based among others on linear fits of the different voltage drops along the current path and the electric field in the arc column over the pulse current. Here, the total voltage u_T was written as a function of the arc current i and the arc length, the length of the current path respectively, l_A:

$$u_T(i, l_{\mathrm{arc}}) = U_{F0} + R_F i + (E_{z0} + \rho_z i) l_{\mathrm{arc}} + (R_{W0} + \rho_W (l_{\mathrm{CTWD}} - l_{\mathrm{arc}})) i \quad (6)$$

The sheath voltage, the sum of the anode and cathode sheath voltage, is represented by a linear function of the current with a constant parameter U_{F0} and a coefficient R_F. The voltage drop over the arc column is described as a linear function of the arc length and the current with a constant field value E_{z0} and an additional coefficient ρ_z. The last term in eqn. (6 represents the voltage drop in the wire dependent on a coefficient ρ_W and the free wire length, which is the difference of the contact-tube-to-workpiece distance (CTWD) l_{CTWD} as a fixed process parameter and the arc length. The coefficients have been deduced from the fitting of measurements, and the model has been proven to be a sufficient approximation in a larger range of process parameters as for pulse currents 300 to 600 A, pulse frequencies between 50 and 130 Hz, pulse durations between 1 and 1.5 ms, wire feed speeds between 3 and 6 m/min and CTWD between 9 and 21 mm. It was deduced for processes with wires of 1.2 mm in diameter and the material mild steel, for the shielding gas Ar+2.5% CO_2 and the flow rate 15 l/min and a welding speed of 30 cm/min. However, a validity also for little different process parameters is expected. The accuracy of the model is demonstrated by the comparison with voltage measurements in Figure 5.

The voltage model (6) requires the knowledge of the arc length as a variable, which is on one hand a deficit of the model. On the other hand, equ. (6) can be easily transformed to determine the arc length $l_{\mathrm{arc}}(u, i)$ as a function of the voltage and current. The possibility of the prediction of the arc length has been also successfully confirmed in [20]. The control of the arc length is an important issue for the welding machine control in the GMAW process to guaranty a stable droplet transfer and therefore the overall process stability. Another benefit of the model is that the different voltage drops can be used to estimate the heat transfer to the wire, which mainly originates from the Ohmic heating in the wire and from the power transfer in the arc sheaths. Details can be found in [21].

Electric model of a short switching arc As a second example, a recent study of a short arc in a commercial low-voltage relay contact [22] is reviewed. The opening of a copper contact system under atmospheric pressure air has been considered in this work for low constant DC currents in the range from 0.5 to 20 A and gap distances up to 6 mm. Besides the voltage measurements, the arc was analysed by high speed imaging and the arc length was determined from image processing. Here, the current path was estimated considering the points of the maximum radiation intensity for every axial position in the gap. An interesting observation was that not only the small regions of the arc attachment at the electrodes show an increased radiation intensity but also a larger region up to approximately 1 mm above the cathode. The measured voltage was plotted as a function of

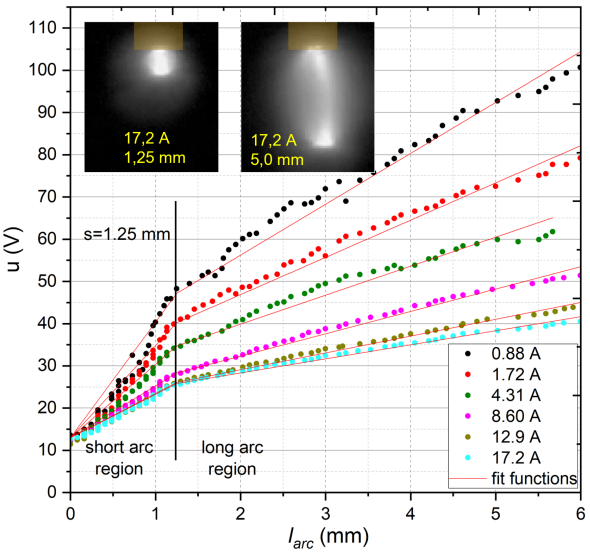

Figure 6. Voltage measurements as a function of the arc length during the opening of a copper contact relay for different DC currents together with examples of arc images for two gap distances.

the arc length as illustrated in Figure 6. An interesting result is that the voltage jumps during the first contact separation are almost similar, which indicates a sheath voltage almost independent of the current. The other important issue is that the voltage increase with the arc length is much higher for small lengths up to approximately 1.25 mm. The change to a lower increase of the voltage with the length occurs approximately at this value of the arc length for all studied currents.

The systematic changes of the voltage with current and arc length found in the experiments have been included in an electric model, where a piecewise linear fit of the voltage increase has been applied to deduce the averaged axial electric field values $E_z = \frac{\Delta u}{\Delta l_{\mathrm{arc}}}$. The voltage fit for vanishing arc length has been considered as a sheath voltage V_0. The electric fields have been deduced both for the near cathode region (up to 1.25 mm) and for the other region for larger arc lengths, respectively. In addition, it turned out that these values show a current dependence which can be expressed by a power law. Finally, an electric model for the voltage has been deduced in the form

$$u(i, l_{arc}) = \begin{cases} U_0 + \frac{a_1}{i^{b_1}} s + \frac{a_2}{i^{b_2}} (l_{\mathrm{arc}} - s) & l_{\mathrm{arc}} \geq s \\ U_0 + \frac{a_1}{i^{b_1}} l_{\mathrm{arc}} & l_{\mathrm{arc}} < s. \end{cases} \quad (7)$$

where U_0, a_1, a_2, b_1, and b_2 are fit parameters, and s =1.25 mm. More details can be found in [22]. The high radiation intensity and the high electric fields in the surrounding of the cathode have been observed in a range much larger than typical sizes on the micrometer scale of the cathode region in existing physical approaches at least for higher currents (see e.g. [23]). This is interpreted as a strong indication for larger deviations from local thermodynamic equilibrium (LTE) in larger parts of the arc in the case of low currents. This hypothesis is confirmed by a recent study of short arcs between copper electrodes at low currents applying a uniform non-LTE model [24].

model	fitted parameters	valid for varying	have to be adapted to
vacuum switching arc	U_d, U_{h1}, U_{h2}, t_0, t_1, t_2, t_3 a, b, c	current, frequency, gap distance, contact speed	electrode geometry and material, pulse shape
copper vapour AC arc	k_{tur}, k_{axmf}, k_{ramf}, k_{net}, b, q, p_0, k_p, k_h	current, frequency	electrode geometry and material, gas and pressure
pGMAW arc	U_{F0}, R_F, E_{z0}, ρ_z ρ_W	current, pulse parameters, wire feed speed, CTWD, welding speed	wire radius and material, shielding gas and flow rate
low voltage DC relay arc	U_0, a_1, b_1, a_2, b_2, s	current, gap distance, contact speed	electrode geometry and material, gas and pressure

Table 1. Fitted parameters of the models and their vailidity.

4. Conclusion and outlook

Four examples of recent studies on electric arc models have been used here to illustrate specific features of such models, in particular

- the possibility to adapt electric models also to a complex voltage behaviour with mode jumps, if the parameter range of the modes can be determined sufficiently - this was shown for a vacuum switching arc exhibiting high-current anode spot modes,
- the inclusion of a more detailed arc power balance in an electric model with the benefit, that main contributions of the power balance and their temporal development can be extracted from the model - this was illustrated for a high-current metal vapour dominated arc,
- the consideration of all relevant voltage drops in the current path including electrode losses and the detailed analysis of arc length and sheath voltages for short high-current arcs - this was shown for the arc in the pulse period of a pulsed gas metal arc welding process,

□ the consideration of a specific voltage behaviour near the cathode in low current arcs - this was demonstrated for a low-voltage relay contact system.

Table 1 gives an overview over the fitted parameters in the four models. The models with unchanged fit parameters are valid for varying operation parameters in the third column. If the properties in the fourth column are changed, then the fit parameters must be re-calibrated by additional measurements. However, this assignment is a rough approach. The operation parameters can be changed in a limited range only, and small changes in the configuration and properties (fourth column) may not require an adjustment of the fit parameters.

It should be mentioned, that the deduction of the more sophisticated electric arc models, as shown here, requires not only voltage and current measurements but optical high-speed diagnostics and arc image processing e.g. to determine the arc length representing the length of the main current path. In addition, some models require at least estimations of the arc temperature or the electrode temperature by spectroscopic or pyrometric methods, respectively.

The developed methods are currently used for the study of other attractive arc applications and to fill further gaps in the knowledge of the electrical characteristics of arcs. One example is the determination of the voltage characteristics of short arcs in hydrogen and nitrogen [25]. Hydrogen, in particular, provides an increased arc quenching behaviour and is used in low voltage DC contactors e.g. for e-mobility [26]. Arcs in hydrogen, methane, and carbon dioxide will become attractive also to applications in the chemical industry. However, corresponding studies are very rare (see e.g. [16]). Beside the use as an electrical heat source to replace the burning of fossil materials, arcs can be used well for an effective dissociation of the molecular gases e.g. for the synthesis of syngas. A challenge for the application in the chemical industry but also for new switching devices would be the operation of the arc at increased pressures of many tens of bars or even higher. The study of such arcs in simple model experiments, e.g. with low arcing times or reduced arc length to reduce the effort, and the deduction of electric models will help to find optimum arc operation parameters and to design appropriate processes and power sources.

References

[1] O. Mayr. Beiträge zur Theorie des Statischen und des Dynamischen Lichtbogens. *Arch. Elektr.*, 37:588–608, 1943.

[2] A. Cassie. Arc rupture and circuit severity: A new theory. *In Proceedings of the Conférence Internationale des Grands Réseaux Électriques à Haute Tension (CIGRE Report), Paris, France*, 102:1–14, 1939.

[3] J. Schwarz. Dynamisches Verhalten eines gasbeblasenen, turbulenzbestimmten Schaltlichtbogens. *ETZ Arch.*, 92:389–391, 1971.

[4] P. Schavemaker and L. van der Slui. An improved Mayr-type arc model based on current-zero measurements. *IEEE Trans. Power Deliv.*, 15:580–584, 2000. doi:10.1109/61.852988.

[5] H. Ayrton. *The Electric Arc.* Cambridge University Press: Cambridge, UK, 2012. ISBN 978-1-108-05268-9.

[6] C. Steinmetz. Electric power into light, Section VI. The arc. *Trans. Am. Inst. Electr. Eng.*, 25:802, 1906.

[7] W. Nottingham. A new equation for the static characteristic of the normal electric arc. *Trans. Am. Inst. Electr. Eng.*, 42:12–19, 1923.

[8] R. Smeets and V. V.Kertesr. Evaluation of high-voltage circuit breaker performance with a validated arc model. *IEE Proc.-Gener. Transm. Distrib.*, 147:121–125, 2000. doi:10.1049/ip-gtd:20000238.

[9] N. Gustavsson. Evaluation and simulation of black-box arc models for high-voltage circuit-breakers, Linköping 2004. arXiv:http://www.ep.liu.se/exjobb/isy/2004/3492/.

[10] R. Ammerman, T. Gammon, P. Sen, and J. Nelson. DC-arc models and incident-energy calculations. *IEEE Trans. Ind. Appl.*, 46:1810–1819, 2010. doi:10.1109/TIA.2010.2057497.

[11] A. Khakpour, S. Franke, R. Methling, et al. An improved arc model for vacuum arc regarding anode spot modes. *IEEE Trans. Dielectr. and Electr. Insul.*, 26:120–128, 2019. doi:10.1109/TDEI.2018.007587.

[12] H. Fink, D. Gentsch, M. Heimbach, et al. New developments of vacuum interrupters based on rmf and amf technologies. *Proceedings ISDEIV. 18th International Symposium on Discharges and Electrical Insulation in Vacuum*, 2:463–466, 1998. doi:10.1109/DEIV.1998.738633.

[13] A. Khakpour, S. Franke, D. Uhrlandt, et al. Electrical arc model based on physical parameters and power calculation. *IEEE Trans. Plasma Sci.*, 43(8):2721–2729, 2015. doi:10.1109/TPS.2015.2450359.

[14] S. St Franke, R. Methling, D. Uhrlandt, et al. Temperature determination in copper-dominated free-burning arcs. *J. Phys. D: Appl. Phys.*, 47:015202, 2014. doi:10.1088/0022-3727/47/1/015202.

[15] A. Khakpour, S. Franke, S. Gortschakow, et al. An improved arc model based on the arc diameter,. *IEEE Trans. Power Del.*, 31:1335–1341, 2016. doi:10.1109/TPWRD.2015.2473677.

[16] P. Gueye, Y. Cressault, V. Rohanio, and L. Fulcheri. A simplified model for the determination of current-voltage characteristics of a high pressure hydrogen plasma arc. *J. Appl. Phys.*, 121:073302, 2017. doi:10.1063/1.4976572.

[17] R. Kozakov, G. Gött, H. Schöpp, et al. Spatial structure of the arc in a pulsed GMAW process. *J. Phys. D: Appl. Phys.*, 46:224001, 2013. doi:10.1088/0022-3727/46/22/224001.

[18] G. Zhang, G. Gött, R. Kozakov, et al. Study of the wire resistance in gas metal arc welding. *J. Phys. D: Appl. Phys.*, 52:085201, 2019. doi:10.1088/1361-6463/aaf5bb.

[19] G. Zhang, G. Gött, R. Kozakov, et al. Study of the arc voltage in gas metal arc welding. *J. Phys. D: Appl. Phys.*, 52:085202, 2019. doi:10.1088/1361-6463/aaf588.

[20] G. Zhang, G. Gött, D. Uhrlandt, et al. A simplified voltage model in GMAW. *Weld. World*, pages 1625 – 1634, 2020. doi:10.1007/s40194-020-00943-x.

[21] G. Zhang, G. Gött, and D. Uhrlandt. Study of the anode energy in gas metal arc welding. *J. Phys. D: Appl. Phys.*, 53:395202, 2020. doi:10.1088/1361-6463/ab93f7.

[22] A. Najam, P. Pieterse, and D. Uhrlandt. Electrical modelling of switching arcs in a low voltage relay at low currents. *Energies*, 13:6377, 2020. doi:10.3390/en13236377.

[23] M. S. Benilov and A. Marotta. A model of the cathode region of atmospheric pressure arcs. *J. Phys. D: Appl. Phys.*, 28:1869, 1995. doi:10.1088/0022-3727/28/9/015.

[24] M. Baeva, V. F. Boretskij, D. Gonzalez, et al. Unified modelling of low-current short-length arcs between copper electrodes,. *J. Phys. D: Appl. Phys.*, 54:025203, 2021. doi:10.1088/1361-6463/abba5d.

[25] A. Najam, R. Methling, J. Hummel, et al. Electrical and optical investigation of an electric arc in hydrogen for short gaps. *Plasma Phys. Technol.*, 10(2):73–76, 2023. doi:10,14311/ppt.2023.2.73.

[26] D. Gonzalez, S. Gortschakow, R. Methling, et al. Switching behavior of a gas-filled model DC-contactor under different conditions. *IEEE Trans. Plasma Sci.*, 48(7):2515–2522, 2020. doi:10.1109/TPS.2020.3003525.